

This work was written as part of one of the author's official duties as an Employee of the United States Government and is therefore a work of the United States Government. In accordance with 17 U.S.C. 105, no copyright protection is available for such works under U.S. Law.

Public Domain Mark 1.0

<https://creativecommons.org/publicdomain/mark/1.0/>

Access to this work was provided by the University of Maryland, Baltimore County (UMBC) ScholarWorks@UMBC digital repository on the Maryland Shared Open Access (MD-SOAR) platform.

Please provide feedback

Please support the ScholarWorks@UMBC repository by emailing scholarworks-group@umbc.edu and telling us what having access to this work means to you and why it's important to you. Thank you.

Using OSSEs to Evaluate the Impacts of Geostationary Infrared Sounders

Erica L. McGrath-Spangler^{a,b}, Will McCarty^c, N. C. Privé^{a,b}, Isaac Moradi^{b,d}, Bryan M. Karpowicz^{b,e}, Joel McCorkel^f



^a *Morgan State University, Baltimore, MD USA* ^b *Global Modeling and Assimilation Office, NASA, Greenbelt, MD USA* ^c *NASA Headquarters, Washington, DC USA* ^d *ESSIC, University of Maryland, College Park, MD USA* ^e *University of Maryland, Baltimore County, Baltimore, MD USA* ^f *Biospheric Sciences Laboratory, NASA, Greenbelt, MD USA*

Corresponding author: Erica L. McGrath-Spangler, erica.l.mcgrath-spangler@nasa.gov

Early Online Release: This preliminary version has been accepted for publication in *Journal of Atmospheric and Oceanic Technology* cited, and has been assigned DOI 10.1175/JTECH D220033.1 The final typeset copyedited article will replace the EOR at the above DOI when it is published.

ABSTRACT: An observing system simulation experiment (OSSE) was performed to assess the impact of assimilating hyperspectral infrared (IR) radiances from geostationary orbit on numerical weather prediction, with a focus on the proposed sounder onboard the Geostationary eXtended Observations (GeoXO) program’s central satellite. Infrared sounders on a geostationary platform would fill several gaps left by IR sounders on polar orbiting satellites, and the increased temporal resolution would allow the observation of weather phenomena evolution. The framework for this OSSE was the Global Modeling and Assimilation Office (GMAO) OSSE system, which includes a full suite of meteorological observations. The experiment additionally assimilated four identical IR sounders from geostationary orbit to create a “ring” of vertical profiling observations. Based on the experimentation, assimilation of the IR sounders provided a beneficial impact on the analyzed mass and wind fields, particularly in the tropics, and produced an error reduction in the initial 24-48 hours of the subsequent forecasts. Specific attention was paid to the impact of the GeoXO Sounder (GXS) over the contiguous United States (CONUS) as this is a region that is well-observed and as such difficult to improve. The forecast sensitivity to observation impact (FSOI) metric, computed across all four synoptic times over the CONUS, reveals that the GXS had the largest impact on the 24-hour forecast error of the assimilated hyperspectral infrared satellite radiances as measured using a moist energy error norm. Based on this analysis, the proposed GXS has the potential to improve numerical weather prediction globally and over the CONUS.

SIGNIFICANCE STATEMENT: The purpose of this study is to understand the impact of the proposed geostationary hyperspectral infrared sounder as part of the Geostationary Extended Observations (GeoXO) program on numerical weather prediction. The evaluation was done using a simulated environment, and showed a beneficial impact on the tropical mass and wind fields and an error reduction in the initial 24-48 hour forecasts. Over the contiguous United States, the GeoXO Sounder (GXS) performed well and had the largest impact of the assimilated infrared satellite radiances on the 24 hour forecast as measured by a moist energy error norm. Based on the results of this study, the proposed GXS has the potential to improve numerical weather prediction.

1. Introduction

The goal of any weather prediction system is to enable better decision making by individuals, industries, and governments. In order to meet this goal, a good, well-performing forecast is required, which benefits from good observations of the atmosphere and its processes. These observations are key to improving model representations of current and future weather conditions. Numerical weather prediction (NWP) systems benefit from conventional and remotely-sensed observations that, when combined with global models through a process called data assimilation, are able to initialize forward in time forecasts.

Although conventional observations, such as radiosondes and ground-based stations, are often-times considered the gold standard and are relatively simple to deploy, their spatial irregularity requires satellite observations to fill the void. The addition of satellite observations to NWP systems have enabled forecasts to be equally skillful in the Northern and Southern Hemispheres (Bauer et al. 2015; Diniz and Todling 2020). This capability is what makes satellite observations the basis for current NWP (Zapotocny et al. 2007).

One of the major types of satellite information for use in data assimilation systems is infrared radiances (Cardinali 2009; Li et al. 2018; Lawrence et al. 2019). Although remarkable progress has been made over the last several decades in terms of spatiotemporal coverage and precision of global observations, gaps in knowledge remain. An option previously used is observations from multispectral channel soundings from geostationary orbit. However, these have limited vertical resolution that is insufficient for many applications (Wang et al. 2007; Schmit et al. 2009).

The other widely available infrared radiance data are from low earth orbit (LEO) from hyperspectral sensors such as the Cross-track Infrared Sounder (CrIS) onboard the Suomi NPP and NOAA-20 satellites, the Atmospheric Infrared Sounder (AIRS) onboard the National Aeronautics and Space Administration's (NASA) Aqua satellite, and the Infrared Atmospheric Sounding Interferometers (IASI) onboard the European Space Agency's (ESA) MetOp satellites. These LEO sounders are essential to NWP by providing high vertical resolution temperature and water vapor information, but are limited both horizontally and temporally (McCarty et al. 2021). The low temporal resolution makes it difficult to view between gaps in the clouds and prevents monitoring of rapidly evolving phenomena that may be of great importance meteorologically and to affected stakeholders (Schmit et al. 2009).

Many of the shortcomings of available satellite infrared radiances would be addressed by the proposed hyperspectral infrared sounder from geostationary orbit. This is a proven concept, having been originally developed by NASA for the Geosynchronous Imaging Fourier Transform Spectrometer (GIFTS) mission concept (Zhou et al. 2002; Velden et al. 2005). The China Meteorological Administration (CMA) launched the Geosynchronous Interferometric Infrared Sounder (GIIRS) in December 2016 (Yang et al. 2017), providing the first geostationary Fourier Transform Spectrometer with high temporal resolution radiances suitable for NWP (Guo et al. 2021). Launched onboard the FengYun-4A (FY-4A) satellite, GIIRS provides observations from a location at 105°E. EUMETSAT has proposed the launch of the Meteosat Third Generation (MTG) hyperspectral infrared sounder (IRS) for 2023 (Holmlund et al. 2021) and the Japan Meteorological Agency (JMA) has plans for launching a follow on to the Himawari program that includes a hyperspectral infrared sounder from geostationary orbit in 2029 (Okamoto et al. 2020; Bessho et al. 2021). The United States' response is the proposed Geostationary eXtended Observations (GeoXO) program that may include hyperspectral infrared observations.

An important methodology to evaluate the impacts of such a proposed instrument system is the use of a set of observing system simulation experiments (OSSEs) (e.g. Atlas et al. 1985; Arnold and Dey 1986; Errico et al. 2013; Hoffman and Atlas 2016). OSSEs allow testing of a new, hypothetical, or proposed instrument that does not have an existing data set in order to provide an assessment of the impact of the new instrument and an estimate of the associated uncertainty.

This is a cost-effective approach to testing proposed observing systems prior to deployment and to optimize the observing strategy and enable rapid assimilation once the real data become available.

Several previous studies have employed hybrid OSSE systems to assess the impact of IR observations from geostationary orbit. A hybrid OSSE combines real observations and numerical weather prediction models or reanalyses so there is no need to represent any of the observations except those from the proposed instrument. This eliminates the need for a nature run and allows evaluation of real events. However, since the truth in a hybrid OSSE system is the real atmosphere and thus unknown, the simulated observations for the proposed instrument must be generated from an NWP model with the associated errors and uncertainties. The simulated observations are therefore not observations of the truth in this system. The information content from the proposed instrument may not be consistent with the information that would be obtained in the real world.

However, hybrid OSSE systems are a useful and less resource intensive methodology for evaluating proposed instruments than a full OSSE framework that utilizes a nature run. For example, Jones et al. (2017) assimilated temperature and humidity retrievals from an IR sensor on a geostationary platform in their experiments representing a severe weather event that produced an Enhanced Fujita-5 tornado. They found a reduction in mid-tropospheric errors relative to an experiment assimilating conventional observations alone and an improved forecast of the helicity. Wang et al. (2021) assimilated geostationary IR radiances and found an improvement in the temperature, moisture, and precipitation representations of two severe storm events. Okamoto et al. (2020) simulated radiances from a proposed geostationary IR instrument as part of the Himawari follow-on program and found improvements in the meteorological fields and typhoon track errors. These studies show the benefit of geostationary IR observations and suggest the utility of a nature run based OSSE framework to further examine the impact within a contained system.

In this study, we examine the impacts of the proposed GeoXO Sounder (GXS), a hyperspectral infrared (IR) sounder, on global data assimilation and NWP using a global OSSE. The global OSSE framework has been developed at the NASA Global Modeling and Assimilation Office (GMAO), and has been extensively validated to ensure realistic performance (Errico et al. 2013; Privé et al. 2021). This framework has been used previously to perform OSSEs for supplemental rawinsondes (Privé et al. 2014), atmospheric motion vectors and infrared radiances (McCarty et al. 2021), and radio occultations (Privé et al. 2022).

This article is organized as follows. Section 2 provides a description of the GeoXO program. Section 3 describes the OSSE and the data assimilation system used. Section 4 discusses the geostationary hyperspectral IR observation generation. Section 5 contains the experiment design, followed by the results in Section 6. A summary and conclusions are given in Section 7.

2. GeoXO Description

The Geostationary Operational Environmental Satellites - R (GOES-R) Series of satellites currently provide advanced imaging, lightning mapping, space weather monitoring, and solar imaging. The GOES-R Series is a four-satellite program that will operate through the mid-2030s. Currently, the National Oceanic and Atmospheric Administration (NOAA) and NASA are developing GeoXO to provide continuity in meeting national environmental sensing requirements for continuous observation of weather and the Earth's environment. GeoXO will improve current observations provided by the GOES-R Series: visible and infrared imagery will have spatial resolution and spectral enhancements, and lightning mapping will have spatial resolution improvements. GeoXO may also include additional capabilities: infrared sounding, night imaging, ocean color imagery, and atmospheric composition measurements.

The GXS, like all hyperspectral infrared sounders, would measure radiation emitted from the atmosphere in thousands of spectral channels. These observations would provide a sounding of the atmosphere with the high vertical resolution necessary for weather forecasting (Schmit et al. 2009) with a temporal resolution high enough to overcome many of the limitations of IR sounders on LEO platforms (Jones et al. 2017; Li et al. 2018; Wang et al. 2021). These channels are sensitive to temperature, water vapor, and trace gases, informing many aspects of atmospheric processes. Such data have been critical to improving the forecasts from modern NWP systems. From the global observation perspective, inclusion of GXS in the GeoXO constellation will further enable meeting The World Meteorological Organization's (WMO) vision of at least five hyperspectral infrared instruments in geostationary orbit by 2040 to form a global "ring" of observations (WMO 2020).

There are many advantages of placing the capability of hyperspectral sounders on a geostationary platform. The high temporal resolution, on the order of 30 minutes, allows more chances to view between clouds while the spatial persistence and horizontal resolution of about 4 km allows the ability to observe weather system development and associated processes, including severe weather.

The lower data latency also allows more rapid assimilation into NWP systems, providing an opportunity to improve atmospheric forecasts (Noh et al. 2020).

3. OSSE Configuration

The OSSE system used by NASA/GMAO has three main components, namely 1) a Nature Run (NR), 2) global observations simulated from the NR that statistically resemble real observations, and 3) a data assimilation system (DAS) to conduct experiments. This system has been extensively tested and verified to ensure robust performance (e.g. Errico et al. 2013; Errico and Privé 2018) and provides a global perspective of the impact of proposed instruments. Importantly, the response of the OSSE system to the assimilation of existing hyperspectral IR instruments well mimics that of the semi-operational system used by the GMAO.

G5NR, the NR used by the GMAO, is a well-validated, 2-year free-running integration of the Goddard Earth Observing System (GEOS) (Rienecker et al. 2008) described by Gelaro et al. (2015). With a horizontal resolution of approximately 7 km and 72 vertical levels from the surface to 0.01 hPa, the simulation starts 1 May 2005 with output every 30 minutes. The free-running model does not represent the actual weather for that time period, but is statistically consistent with the physical atmosphere. For an OSSE framework, the NR is considered the "truth" from which observations are simulated and against which the analyses and forecasts may be verified. This means that the "truth" is completely known and errors can be calculated explicitly.

The Nature Run is sampled at the spatiotemporal locations of actual observations, from June to September 2015 in order to generate the simulated observations (Errico et al. 2017). This is in order to mimic the observing system available in 2015. The observations assimilated in the control are listed in Table 1. Each observation type is generated from the NR differently, according to the methods described in Errico et al. (2017). Radiance data types are affected by the cloud fields of the NR for quality control purposes so that the distribution of observations reflects the atmospheric state of the NR. The geostationary infrared radiance observations that are the focus of this study are described in Section 4.

Realistic errors are added to the synthetic observations following Errico et al. (2017). Both correlated and uncorrelated random errors are added in order to better approximate real errors that originate from instrument errors, representativeness errors, and errors in the way the data

TABLE 1. List of observations assimilated in the control.

Instrument Type	Instrument
Conventional	Radiosonde, Surface, and Aircraft
Ground Retrieved	NEXRAD Winds and Wind Profilers
Satellite Retrieved	Geostationary AMV SEVIRI (<i>Meteosat-10</i> ; <i>Meteosat-8</i>) AHI (<i>Himawari-8</i>) GOES Imager (<i>GOES-13</i> ; <i>GOES-15</i>) Polar AMV MODIS (<i>EOS Terra</i> ; <i>EOS Aqua</i>) Scatterometer ASCAT (<i>MetOp-A</i>) Radio Occultation Bending Angle COSMIC GRAS (<i>MetOp-A</i> ; <i>MetOp-B</i>)
Satellite Radiance	Infrared IASI (<i>MetOp-A</i> ; <i>MetOp-B</i>) CrIS (<i>SNPP</i>) AIRS (<i>EOS Aqua</i>) HIRS (<i>MetOp-A</i>) Microwave Temperature AMSU-A (<i>NOAA-15</i> ; <i>NOAA-18</i> ; <i>NOAA-19</i> ; <i>MetOp-A</i> ; <i>MetOp-B</i> ; <i>EOS Aqua</i>) ATMS (<i>SNPP</i>) SSMIS (<i>F17</i>) Microwave Humidity MHS (<i>NOAA-18</i> ; <i>MetOp-A</i> ; <i>MetOp-B</i>) ATMS (<i>SNPP</i>)

assimilation process handles observations since simulated observations tend to have less intrinsic error than in reality. This addition of errors differs based on the instrument and is done so that the magnitude and correlation length scale are adjusted to match the statistical metrics of real observations.

The DAS used for the experiments combines a more modern version of the GEOS (Molod et al. 2015) than was used to compute the G5NR with the Gridpoint Statistical Interpolation (GSI) described by Wu et al. (2002) and Kleist et al. (2009). The model was run on a cubed sphere dynamical core (Lin 2004; Putman and Lin 2007) with 72 vertical levels that transition from terrain following near the surface to pure pressure levels aloft. The ensembles used for calculation of background error for the hybrid 4DEnVar are taken from the baseline run described by Privé

et al. (2022) to reduce computational expense. Satellite radiances were assimilated using the Community Radiative Transfer Model (CRTM) (Han et al. 2006; Chen et al. 2008).

Several choices were made to maximize differences between the NR and the version of GEOS used in the experiments in order to optimize the realism of the observation impacts seen in the OSSE. Principally, the microphysical convection scheme was changed from the default single moment (Bacmeister et al. 2006) used in the NR to the more sophisticated two-moment scheme described by Barahona et al. (2014). This change is most impactful in frequently convective regions in the tropics and the midlatitudes of the summer hemisphere. Additional changes included an adjustment to a relative humidity threshold and a different version of the boundary layer parameterization, which will impact estimates of the inversion height. Combined, these changes introduced a model error between the NR and the DAS model meant to mimic model errors when assimilating real observations, reducing some of the suboptimality of using an identical model for the NR and the experiments (Privé and Errico 2013).

The impact of GXS observations is particularly of interest over the contiguous United States (CONUS) and therefore a validation of the OSSE system in this region was performed. The observation impact between the OSSE system and a system assimilating real observations was evaluated using the forecast sensitivity observation impact (FSOI) metric (Langland and Baker 2004; Zhu and Gelaro 2008; Gelaro and Zhu 2009) for once-daily forecasts during July. Moist energy error norms for the 24-hour forecasts were computed for the CONUS region (defined here as between 20°N and 52°N latitude and between 130°W and 60°W longitude) and are shown in Figure 1. For the net FSOI, a negative value indicates a reduction in the 24-hour forecast error due to the observation. The error reduction in the real case is larger than in the simulated environment of the OSSE on the right side of Figure. 1, most likely due to insufficient model error in the OSSE (Privé and Errico 2019). Over the CONUS, it is notable that the impacts of hyperspectral infrared instruments (AIRS, IASI, and CrIS) in the OSSE system well represent the impacts observed in the real system used semi-operationally by the GMAO. In the FSOI metric for both the real and OSSE simulations shown in Figure 1, the AMSU-A observations have the greatest impact, consistent with previous studies (Zapotocny et al. 2008), however, over the relatively small CONUS region, the AMSU-A impact in the OSSE system is weaker than in the real system. The differences between the Real and OSSE impacts should be borne in mind when interpreting the results of the experiments.

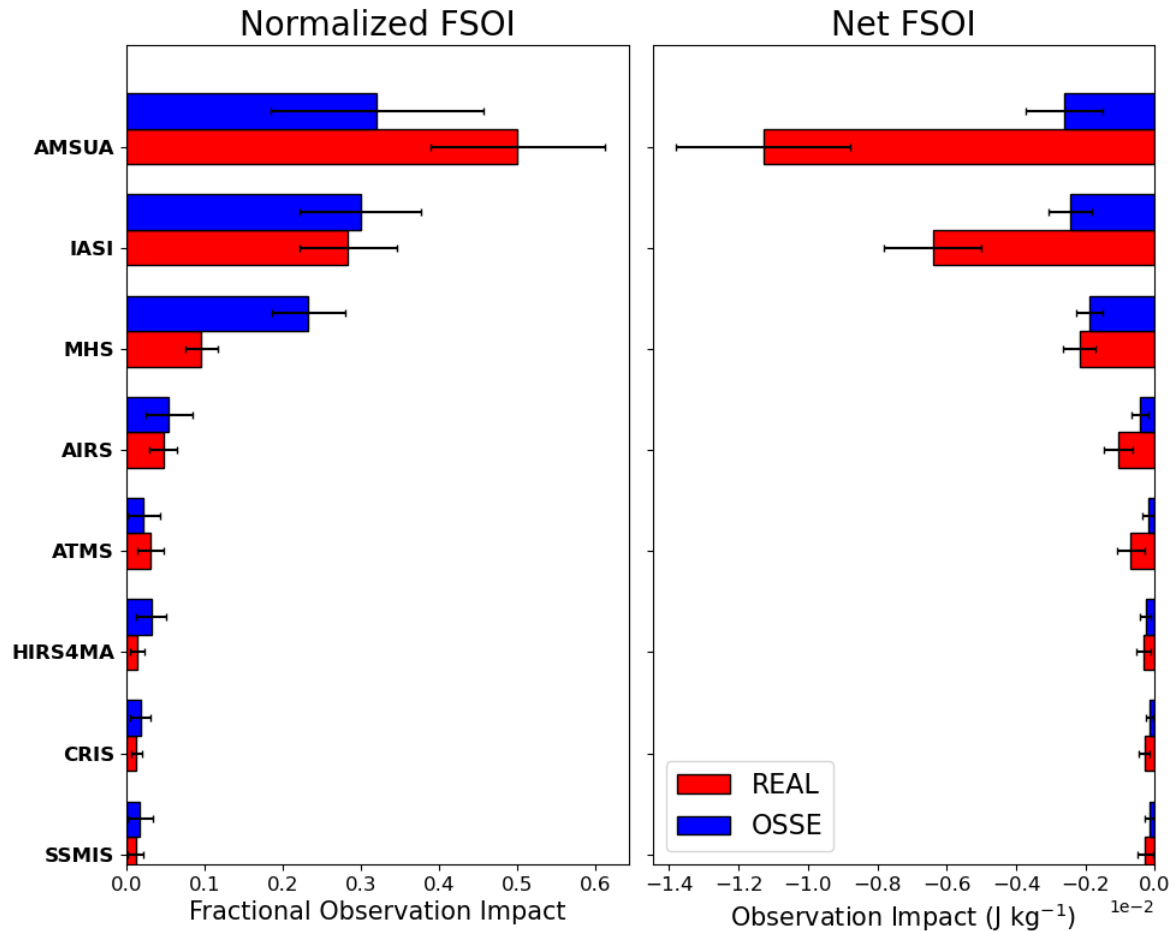


FIG. 1. (left) Observation impact as a function of satellite radiance instrument, normalized by the sum of all instruments, from adjoint calculations using moist energy error norm for the real (red bars) and OSSE (blue bars) simulations, computed over the CONUS region. (right) The same, but showing the net impact, J kg^{-1} .

4. Hyperspectral IR Observations from GEO

Hourly observations for four hypothetical Geostationary Infrared Sounders (GEOIRS) were generated for this study. Of these, one is the proposed GXS that is part of the GeoXO program, with a satellite subpoint of 105°W . However, all four satellites are identical with the satellite subpoint being the only difference among them: the simulated channels are the same for all the GEOIRS instruments. The channels were selected based on specifications for the proposed Infrared Sounder (IRS) hyperspectral instrument onboard the Meteosat Third Generation (MTG) satellite. The GEOIRS observations were estimated using a range expanded beyond IRS to accommodate potential changes to the proposed instrument with 2960 channels and a spectral

wavenumber resolution of 0.625 cm^{-1} , operating from 650 cm^{-1} to 2500 cm^{-1} . Currently, the proposed channels for GXS range from 680 cm^{-1} to 2250 cm^{-1} . The synthetic observations for this study were generated using the GMAO OSSE for Weather Analysis Software Package version 3.x (GOWASP, Errico et al. 2017).

GOWASP requires the location and time of the observations as input in order to sample required geophysical variables such as temperature, water vapor, ozone, clouds, and pressure from the G5NR. The GEOIRS observation locations were generated based on the GOES-R coverage, relocated to the satellite subpoints associated with the four GEOIRS instruments at 140°E , 105°E , 0° , and 105°W and discussed further in Section 5. After reading the location and time of the observations, the required surface and atmospheric profiles are then interpolated from the G5NR to the corresponding time and location of the desired synthetic observations. These profiles are input into the CRTM version 2.2.3 to simulate the synthetic observations. Although a different radiative transfer model would ideally be used to generate the observations from what is used to assimilate them to allow the inclusion of observation operator errors, this study focuses more on the information content of the GEOIRS observations and a future study will further examine the effect of observation errors, including those from the operator.

GOWASP accounts for the cloud contamination using probabilistic methods (Errico et al. 2017) to create realistic spatiotemporal distributions of observations that reflect the NR cloud fields. The process ensures that cloud contaminated channels are rejected by the quality control process and not assimilated in the DAS. In order to reduce the computational demand, the high resolution IR radiances are partially thinned before being simulated by GOWASP, with cloud contaminated observations being preferentially discarded as described in Section 3.1.2 of Errico et al. (2017). This thinning technique is similar to that of the DAS, but is less severe.

In order to reduce redundancy and correlations in spectral space that are not accounted for in the data assimilation system, as well as to avoid sensitivities to unrepresented constituents, only a subset of the channels are assimilated. In total, eighty-five channels were selected for assimilation across the total observed range. Seventy temperature sounding channels were used, ranging from 650 cm^{-1} to 980 cm^{-1} and fifteen water vapor channels were used, ranging from 1765 cm^{-1} to 2005 cm^{-1} . Only those channels that are assimilated by the DAS are simulated with GOWASP.

The lower cutoff for the proposed spectral range of GXS is currently 680 cm^{-1} , resulting in 20% of the channels selected for assimilation being outside the range of GXS.

A Principal Component Analysis conducted on an ensemble of simulated observations revealed approximately 140 pieces of information in spectral space. For the longwave infrared temperature sounding channels along with the $11\text{ }\mu\text{m}$ window channels, the channel selection from AIRS in the DAS was leveraged selecting the nearest channel available on the GEOIRS for the assimilation. Typically, the longwave side of the $6\text{--}7\text{ }\mu\text{m}$ water vapor absorption feature is used in the DAS, however, owing to more pieces of information present in the shortwave side, fifteen channels were selected minimizing inter-channel correlation. Additionally, the $9.6\text{ }\mu\text{m}$ ozone absorption band was avoided, along with other trace constituents which are poorly represented in the DAS. The $4\text{ }\mu\text{m}$ CO_2 absorption band was also avoided due to uncertainties in its simulation.

The channel selection balanced the minimization of inter-channel correlation while preserving high vertical profiling resolution of the atmosphere. The vertical sampling is shown in Figure 2, where bold points represent selected channels at each channel's weighting function peak (derivative of transmission with respect to altitude) assuming a US Standard Atmosphere. This is consistent with the procedure used for most hyperspectral infrared instruments (McNally et al. 2006; McCarty et al. 2009; Reale et al. 2018; McCarty et al. 2021). Some channels, indicated by blue points on Figure 2, were assimilated in this study, but are outside of the proposed spectral range of the GXS instrument. The assimilated channels were chosen based on the selection of AIRS channels assimilated in the GMAO system and those outside of the spectral range of GXS primarily sample the stratosphere with weighting function peaks at pressures aloft of 100 hPa. Section 6 therefore excludes stratospheric results at these levels though this does not entirely eliminate the effects of these channels as the tail of these weighting functions extend downward to 300 hPa.

The GEOIRS observations do not have errors explicitly added for several reasons including that the error magnitude is unknown since the instrumentation is still in development and uncertainty exists in its estimation. However, some implicit error can be assumed. Two implicit errors are representativeness error due to different resolutions between the high-resolution G5NR and the comparatively lower resolution DAS, and error from high cloud contamination. More general information about the observation generation and the associated errors may be found in Errico et al. (2017).

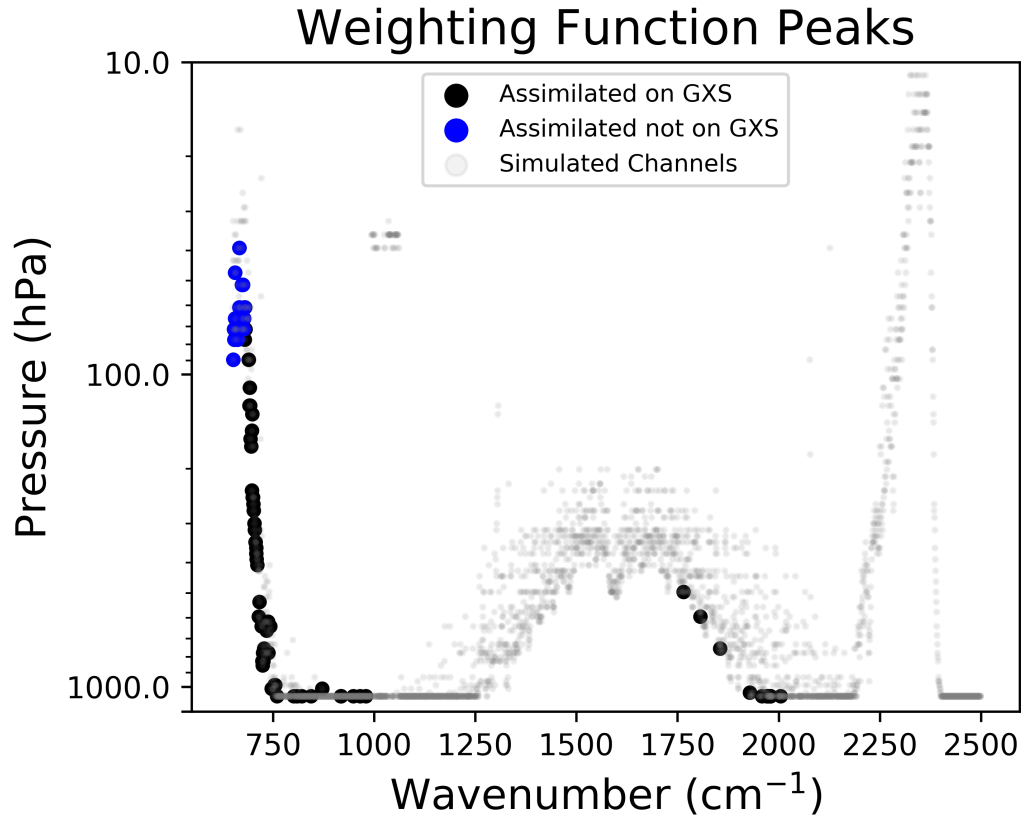


FIG. 2. Weighting function peaks for each channel in GEOIRS instruments. Large bold points represent assimilated channels, while small grey points represent unused instrument channels. The blue points are assimilated channels that will not be included in the proposed GXS instrument.

5. Experiment Design

A control run is made to act as the baseline for comparison with the experiment run. The list of observations assimilated in the control simulation is available in Table 1. A permutation of the control, the 4-Sat experiment, assimilated all of these observations plus radiances from four geostationary hyperspectral infrared instruments generated as specified in Section 4. Both experiments simulated the period 1 July through 31 August 2006, with a spin-up period beginning June 26th. The analysis was generated at $0.25^\circ \times 0.3125^\circ$ horizontal resolution using a 6 hour assimilation window and a hybrid 4-dimensional ensemble variational (hybrid 4DEnVar) assimilation scheme (Todling and El Akkraoui 2018). Seven-day forecasts were initialized at 0000 UTC from 1 July to 31 August 2006 and run at the same resolution as the analysis. The radiance bias coefficients

were spun up for a multi-week period during the calibration process. The calibration is an iterative process, separate from the spin up, that adjusts the OSSE system to mimic the real system and adjusts the simulated errors and cloud probability functions of the existing observation types to match those in the real world.

For the 4-Sat experiment, the four geostationary infrared sounders assimilated are identical in terms of radiance channels, with the only variable being the satellite subpoint used. These were selected as 140°E, 105°E, 0°, and 105°W, corresponding to the satellite subpoints of Himawari, FY-4A, MTG, and the proposed NOAA/NASA GXS respectively. An example of the satellite coverage is provided in Figure 3 with the selected channels for these instruments illustrated in Figure 2. The GEOIRS observations were assimilated hourly using a thinning of 180 km, consistent with the other IR sensors from polar-orbiting satellites. Cloud detection was performed by the GSI as done in Eyre and Menzel (1989). Variational bias correction is applied to the GEOIRS radiances and observation errors used in the assimilation procedure and is done in a method that is consistent with other infrared satellite radiances.

6. Results

The addition of a new instrument may affect the performance of an experiment in multiple ways. Results from the assimilation of geostationary hyperspectral infrared instruments are therefore presented in three separate categories. The first is the performance of the data assimilation procedure and the resulting analysis. Second, the impact of GEOIRS assimilation on the NWP forecasts is described. The third category examined here is an assessment of the observation impact in the context of the FSOI metric (Langland and Baker 2004; Zhu and Gelaro 2008; Gelaro and Zhu 2009). In an effort to show results from the GEOIRS instruments only within the proposed spectral range of the GXS, only pressures greater than 100 hPa are shown. The FSOI results were computed without the inclusion of the channels outside the GXS range.

a. Analysis results

Unlike in the real atmosphere, the "truth" is known in an OSSE and takes the form of the nature run. Therefore, aside from differences in resolution, the analysis error can be computed directly and perfectly.

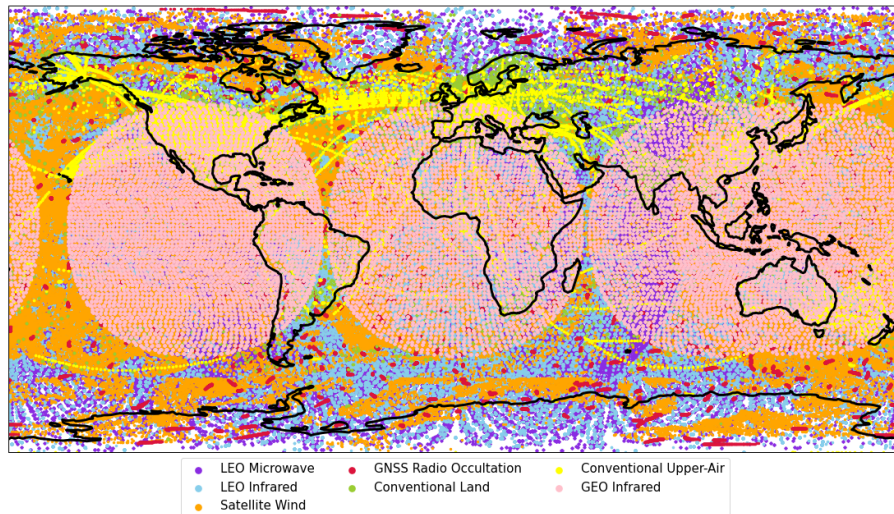


FIG. 3. All observations assimilated in the OSSE for a six hour period centered upon OSSE time 0000 UTC on 1 Aug 2006. The observations are classified into low earth orbit (LEO) Microwave (purple), LEO Infrared (light blue), Satellite-derived winds (orange), Global Navigation Satellite System (GNSS) Radio Occultation (red), Conventional Land (green), Conventional Upper-Air (yellow), and geostationary earth orbit (GEO) Infrared (pink).

A map of the root mean square analysis error differences is shown in Figure 4 at two different levels for temperature, specific humidity, and zonal wind. Temperature is directly impacted by the assimilation of hyperspectral IR radiances and this field shows a distinct impact of GXS assimilation at 312 hPa with an oceanic signal that is largely an improvement north of approximately 30°S. At the lower level, the strongest signal is mostly over the Pacific Ocean, off the west coast of South America, showing an improvement in the 4-Sat experiment. For specific humidity, the more organized signal is at 857 hPa with a degradation in the 4-Sat experiment over South America, potentially related to the difficulty in assimilating infrared radiances over land regions with high heterogeneity, and in the cloud deck region off the west coast of North America though there is an improvement off the coast of South America. The zonal wind response at these levels is more mixed.

The zonally averaged root mean square error of the analysis temperature for the control and the difference between the 4-Sat experiment and the control, normalized by the control, is shown

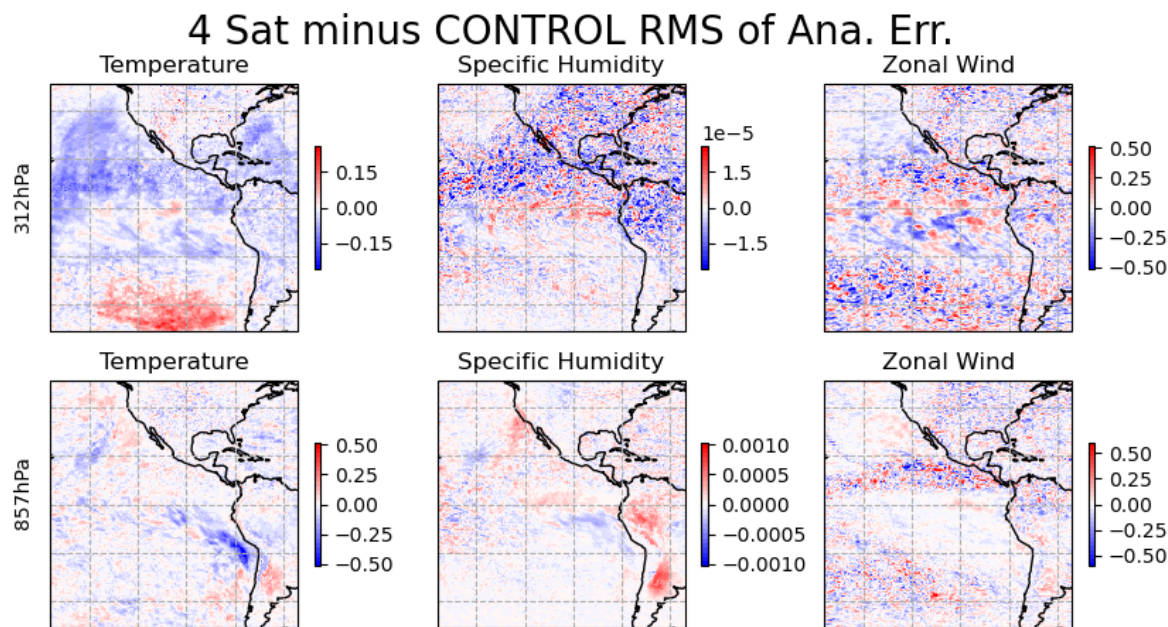


FIG. 4. Difference of root mean square error for the 4-Sat minus the control analyses for (left) temperature (K), (middle) specific humidity (kg kg^{-1}), and (right) zonal wind (m s^{-1}) at (top) 312 hPa and (bottom) 857 hPa. The domain is restricted by the region observed by the GXS instrument (approximately 156°W to 54°W longitude and equatorward of 51°).

in Figure 5. The leftmost plots are for the Global region, the middle plots show the error for the latitudes and longitudes spanned by the GXS observations (approximately 156°W to 54°W longitude and equatorward of 51°), and the rightmost plots show the error for the CONUS, defined here as between 20°N and 52°N latitude and between 130°W and 60°W longitude.

From the control, it is obvious that much of the error is present in the lower troposphere, below approximately 800 hPa. The arc of enhanced error from the equator, extending southward toward Antarctica is associated with the low cloud deck over the cold ocean close to the western coast of South America and is further emphasized when examining the smaller region defined by the GXS.

Examining the impact of assimilating the geostationary hyperspectral infrared instruments in the 4-Sat experiment in the lower panels of Figure 5, a modest temperature improvement is present in the tropics with a maximum tropical improvement on the order of 8% at 300 hPa. As seen in Figure 4, the degradations south of approximately 30°S are off the west coast of South America. It

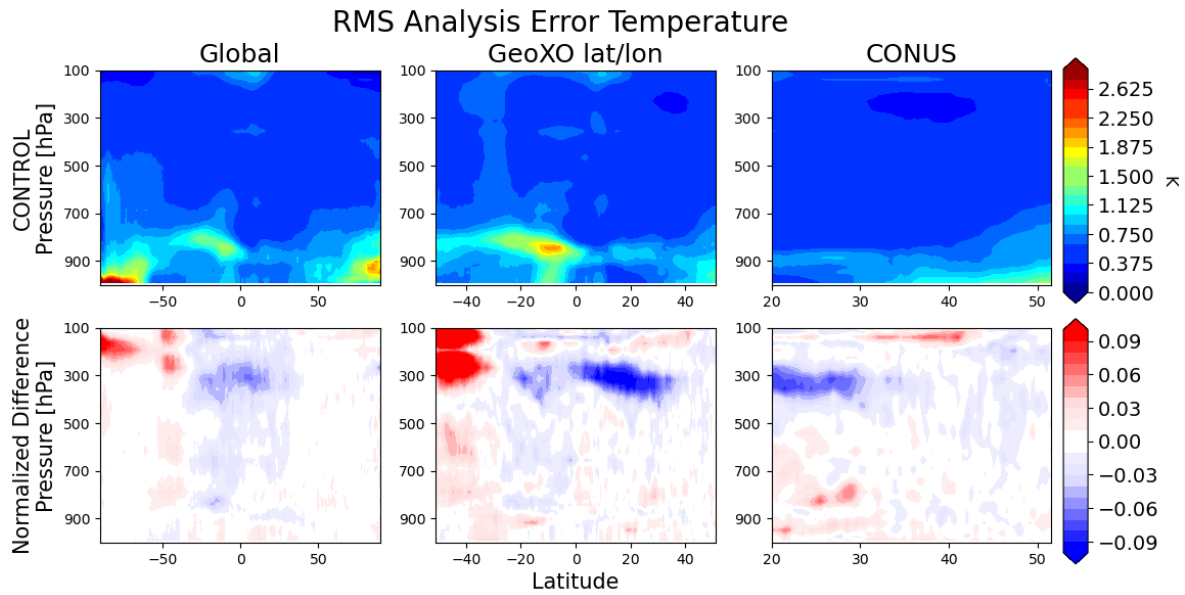


FIG. 5. (top) Zonal root mean square error for temperature (K) in the control vs. the nature run for the (left) global, (middle) GXs defined latitudes and longitudes, and (right) CONUS regions. (bottom) The normalized fraction change in RMSE relative to the control in the 4-Sat experiment. Blue or red indicates an improvement or degradation, respectively, by the addition of the geostationary IR radiances.

is expected that the largest temperature improvement occurs in the tropical region because that is the broadest area observed by the geostationary satellite infrared radiances.

Focusing on the smaller region determined by the latitudes and longitudes observed by the GXs instrument in the center panels of Figure 5, the temperature error in the control is generally larger than it is globally. This is due to the stronger influence of small, variable regions, such as off the South American coast, that contribute to uncertainty in the simulations. In this smaller region, the inclusion of hyperspectral infrared radiances from geostationary orbit leads to an upper tropospheric temperature improvement from roughly 30°S to 40°N. A degradation is present south of 30°S that is also enhanced in the smaller domain.

The region surrounding the contiguous United States is of prime importance to the GeoXO program as one of its' aims is to improve weather prediction in this region. CONUS is heavily observed, resulting in generally low error in the control simulation. However, the predominance of land within the CONUS domain leads to a near surface error. The effect on the analyzed temperature is largely neutral north of about 30°N, consistent with the impact globally, but there is

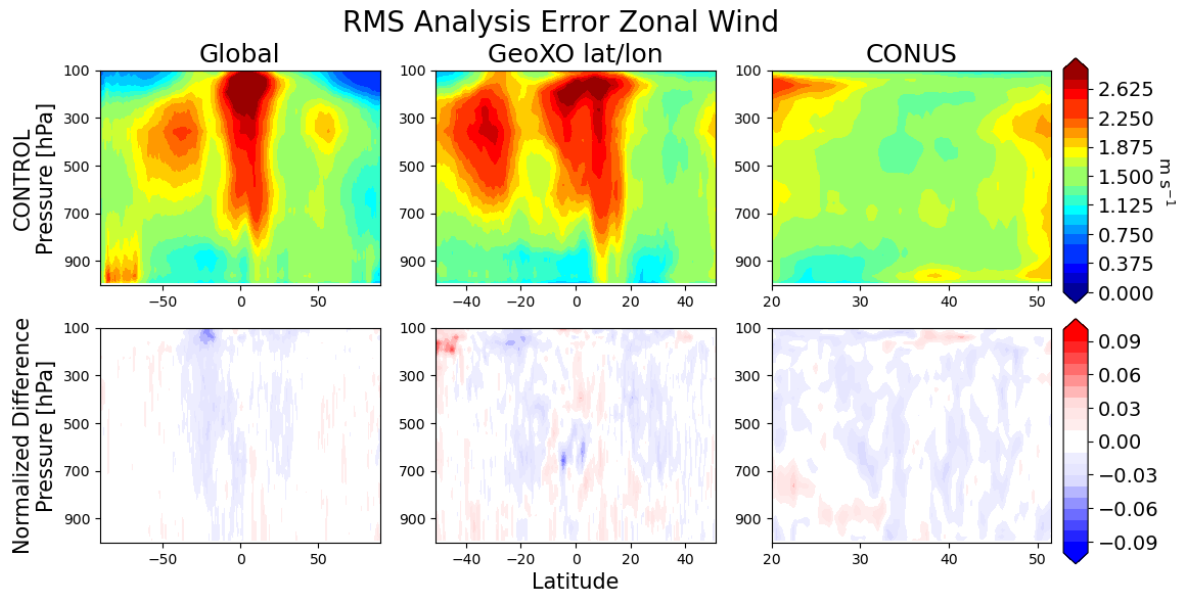


FIG. 6. Same as Figure 5, but for zonal wind (m s^{-1}).

a noticeable improvement in the upper troposphere south of this latitude. The slight degradation in the lower tropospheric temperature is spatially located over the ocean off the west coast of North America, potentially related to the difficulties in properly representing the stratocumulus clouds in this region that are affected by differences in the DAS microphysics and boundary layer parameterizations.

A major advantage of a hyperspectral infrared instrument on a geostationary platform is the ability of the instrument to observe phenomena as they evolve with high temporal resolution. This low latency translates to data on the winds, thereby providing new information content to the data assimilation system. Although the wind is not directly observed by the GXS, wind increments may be inferred through covariances between the wind and variables that are directly observed by GXS in the data assimilation system.

Figure 6 shows the zonally averaged root mean square analysis error for zonal wind. Errors in the control are consistent with locations of the midlatitude and tropical easterly jets. The inclusion of the new information content from the infrared radiance assimilation results in a widespread improvement in the estimate of the analyzed zonal wind equatorward of the midlatitude jets and in the descending branch of the Hadley Circulation.

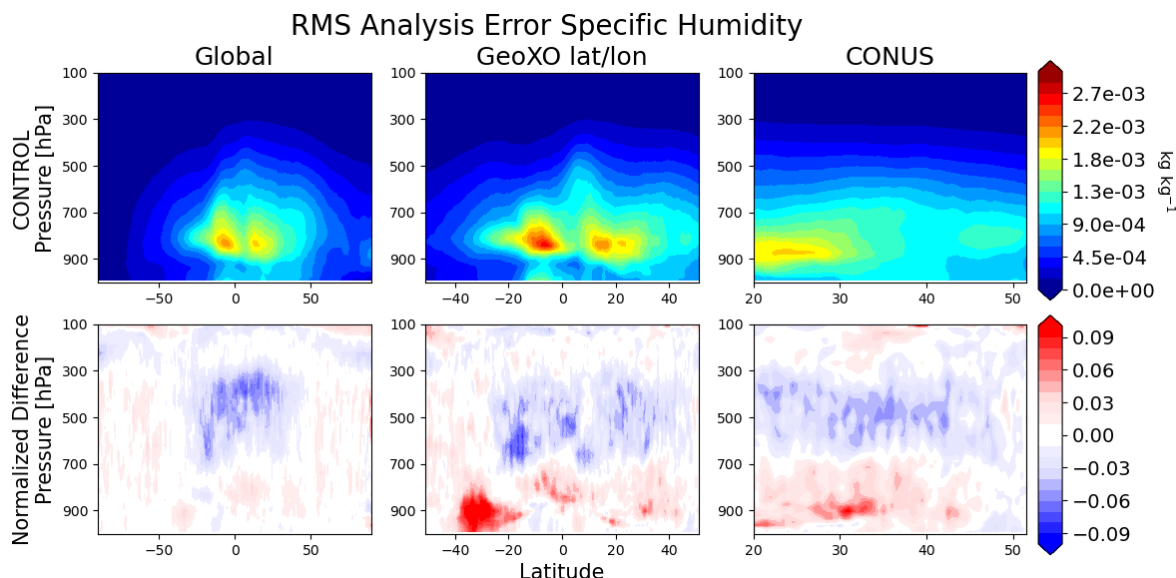


FIG. 7. Same as Figure 5, but for specific humidity (kg kg^{-1}).

Focusing on the latitudes and longitudes defined by the GXS, the result is more mixed, but the improvement in zonal wind generally remains. Over the smaller CONUS region, the zonal wind improvement is widespread throughout the column as a testament to the benefits of high temporal resolution observations over this region.

Improving temperature and wind estimates can contribute to an improvement in tracer transport and therefore in atmospheric concentrations of these variables. The improved tracer concentrations can, in turn, provide positive feedback by contributing valuable wind information. These impacts on specific humidity are examined in Figure 7. The largest errors in specific humidity in the control exist in areas where water vapor content is high, namely within the tropical column and in regions of high cloud content.

In these experiments, fifteen water vapor channels from the GEOIRS observations are assimilated that are sensitive to both temperature and water vapor. Globally, the impact of assimilating hyperspectral IR is an improved representation of specific humidity in the analysis, particularly in the free troposphere and in the tropics. This partially results from an improved representation of the wind and temperature fields due to the added information content from the high resolution observations from geostationary orbit.

In the region observed by the GXS instrument, the free tropospheric specific humidity is improved on the order of 5%. The near surface degradation at approximately 30°S results from enhanced

error over South America with the weak degradations further north resulting from errors off the west coast of the Americas, perhaps related to inconsistencies in estimates of cloud properties between the DAS and the G5NR due to the different parameterization choices made to increase model error realism. This result persists over CONUS with an improved analysis of specific humidity in the free troposphere from approximately 650 hPa to 300 hPa and a slight degradation closer to the surface, mostly confined to the eastern Pacific region where there is a strong low-level inversion that is difficult for the DAS to represent due to sharp gradients and the broad length scale of the increments associated with the assimilated observations. This issue is not particular to the GEOIRS observations.

These analysis results directly impact the predictive skill of the subsequent forecasts as they are used for initialization. An improved analysis provides improved initial conditions for the forecasts, a necessary condition for the production of better weather forecasts.

b. Forecast results

Anomaly correlation of 500 hPa geopotential height was examined in both the Northern (20°N to 80°N) and Southern (80°S to 20°S) Extratropics (not shown). There were no significant differences between the control and 4-Sat experiments in the Northern Hemisphere. In the Southern Hemisphere, there was a small, significant improvement in the short-range forecast anomaly correlation that degraded with time.

Figure 8 shows the change in temperature root mean square error as a function of pressure and forecast time with forecasts validated against the G5NR. The top row shows the time evolution of error in the control simulation and the bottom row shows the normalized difference of the 4-Sat experiment from the control. As expected, as time increases so does the error, consistent with results from real forecasts.

In the global domain, temperature improvements occur in the 4-Sat experiment throughout the troposphere out until approximately day 2. Later, the forecast results convert so that the 4-Sat experiment performs worse than the control. Although the degradation is generally not statistically significant, it shows that the positive impact of the improved initial conditions weakens as model error and chaotic error growth begin to dominate the effects of the improved initial conditions. This is consistent with other work (e.g. Privé and Errico 2013; Cucurull and Casey 2021; Privé et al.

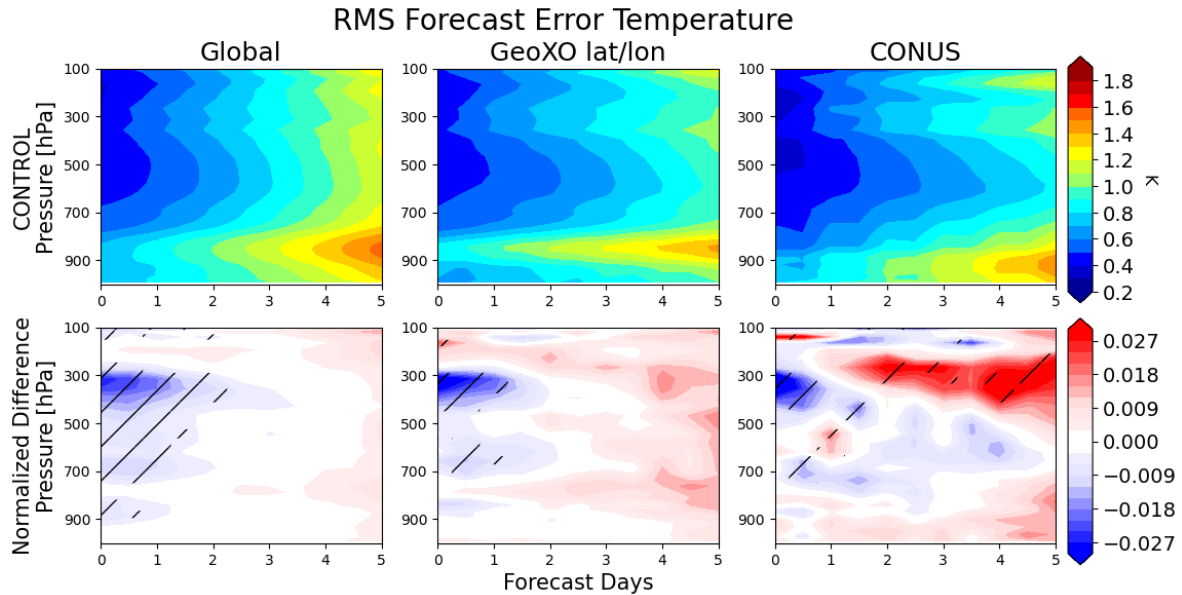


FIG. 8. (top) Root mean square temperature error as a function of pressure and forecast time for the (left), (middle) GXS defined latitudes and longitudes, and (right) CONUS regions in K. (bottom) Normalized fraction change in RMSE relative to the control in the 4-Sat experiment. Blue or red indicates an improvement or degradation, respectively, by the addition of the geostationary IR radiances. Hatch marks indicates significance at the 90% level.

2022) that generally finds the largest impacts occur during the early forecast period, especially over the tropics and summer hemisphere.

In the smaller domain defined by the GXS observed latitudes and longitudes, the tropospheric temperature improvement is again confined to the mid-troposphere, but is more intense at approximately 300 hPa with the time of significant improvement reduced to approximately 1.5 days. Over CONUS, the small domain results in statistics that are mixed with an improved temperature forecast between 400 hPa and 300 hPa for about a day. After that time frame, the response is more negative as the forecast model error increases with time.

Figure 9 shows the forecast results for the zonal wind. As with the temperature, the control forecast error grows with time for each domain as the simulation progresses, with greatest error growth in the upper troposphere. Globally, the added temporal information from the geostationary platform produces an improvement throughout the troposphere extending to 2 days in the mid-

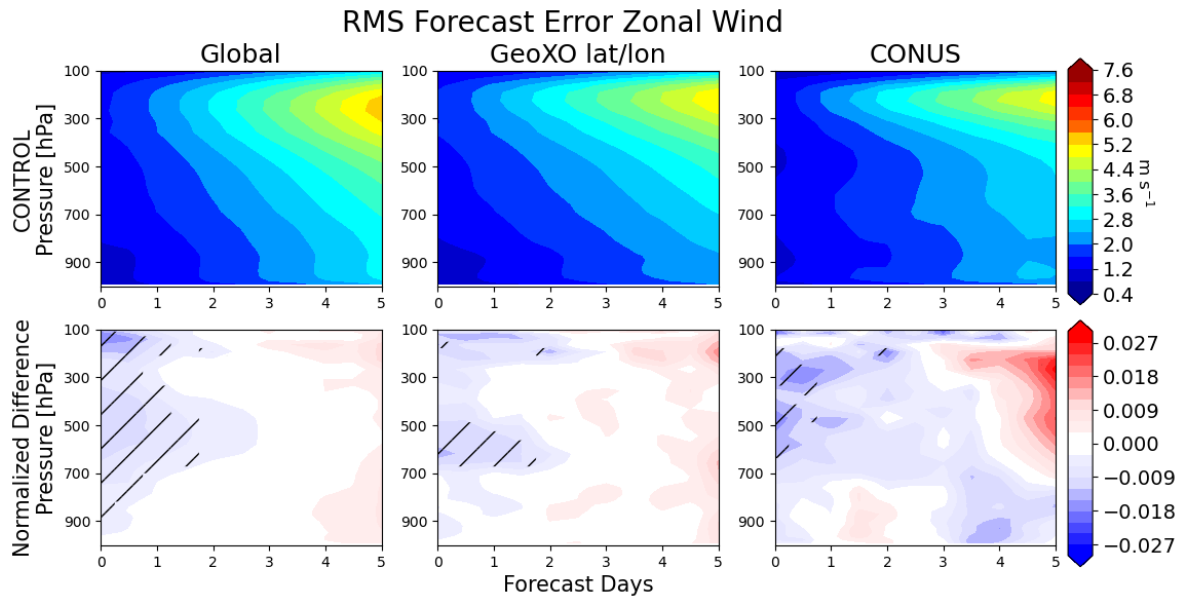


FIG. 9. Same as Figure 8, but for zonal wind in m s^{-1} .

troposphere. The improvement shows the consequence of adding this new information and some of the potential for this proposed instrument.

Focusing on the two smaller domains examined here, the improvement is maintained though not as widespread. For the GXS domain, a significant, but small in magnitude wind improvement is present in the mid-troposphere at about 600 hPa. Over CONUS, the significant improvement is present in the upper troposphere, from about 600 hPa to 200 hPa. It is particularly consequential that such an improvement is present over the CONUS since improvements in this well-observed region are difficult to achieve.

The impact of the improved winds and temperature has repercussions for the water vapor distribution through improved representation of advection and through cross correlations in the data assimilation scheme between the improved temperature and water vapor. Figure 10 shows the control specific humidity forecast error and the improvement produced by the assimilation of geostationary IR radiances in the 4-Sat experiment. In the control, the forecast error is largest at approximately 800 hPa and grows with time. This height is consistent with low-level clouds, particularly those off the west coast of continents that tend to have a lot of uncertainty that is difficult to capture with a model.

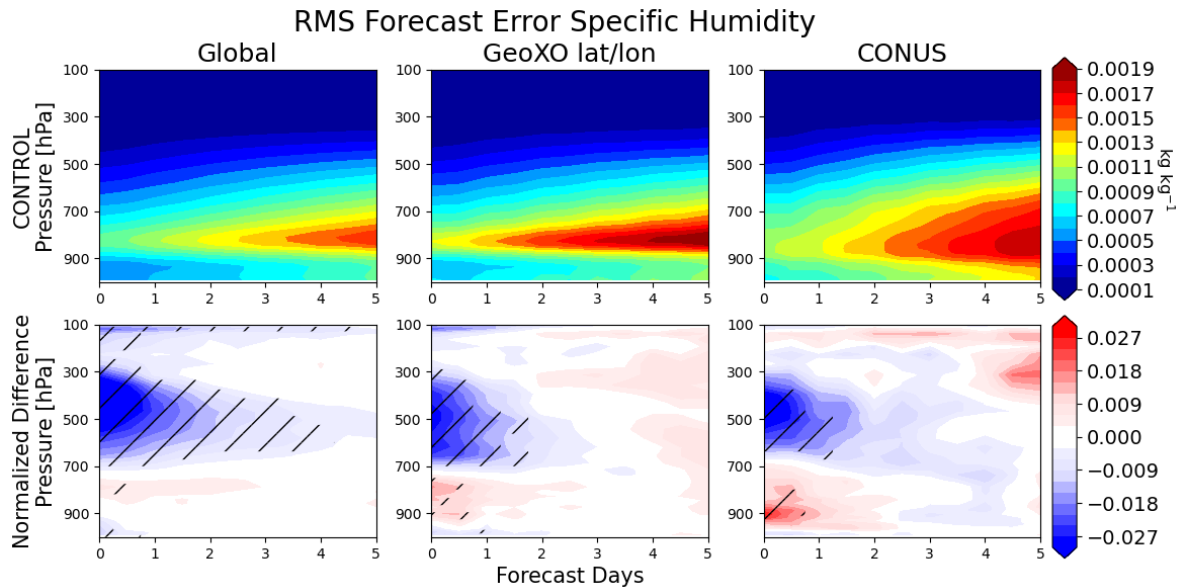


FIG. 10. Same as Figure 8, but for specific humidity in kg kg⁻¹.

There is a significant improvement in the estimate of global tropospheric specific humidity in the 4-Sat experiment from 700 hPa and aloft that extends to 4 days that has implications for entrainment. A slight degradation occurs around 800 hPa, the level of largest error in the control. On the smaller domains, the mid-tropospheric specific humidity improvement is still present, though smaller as the domain size decreases. These improvements extend to 2 day forecasts.

c. FSOI results

It is possible to characterize the impact of hyperspectral IR radiances from geostationary orbit using the FSOI metric (Langland and Baker 2004; Zhu and Gelaro 2008; Gelaro and Zhu 2009). This metric quantifies how each observation impacts the 24 hour forecast moist energy error norm (Ehrendorfer et al. 1999; Holdaway et al. 2014). This should not be considered a strict ranking of instrument impact on error reduction, but generalized groupings of high-impact instrument types may be made.

The global FSOI, examining only satellite radiances, is shown in Figure 11. These results show the 24 hour error impact for the 0000 UTC forecasts only and it is apparent that polar orbiters generally perform better than observations from geostationary orbit using this global metric. This is due to polar orbiters always sampling somewhere in the domain and are capable of observing

the full globe. Since observations are always occurring within the domain, the disadvantage of only sampling a given area twice a day is not strongly felt by this metric and all observations are capable of impacting the error calculation. Among the geostationary infrared sounders, the GXS instrument performs well, roughly in the middle based on this metric. Globally, the GXS performs more poorly than the polar orbiting satellites because it is incapable of observing regions outside its specified domain and therefore cannot directly impact error reduction in areas far away.

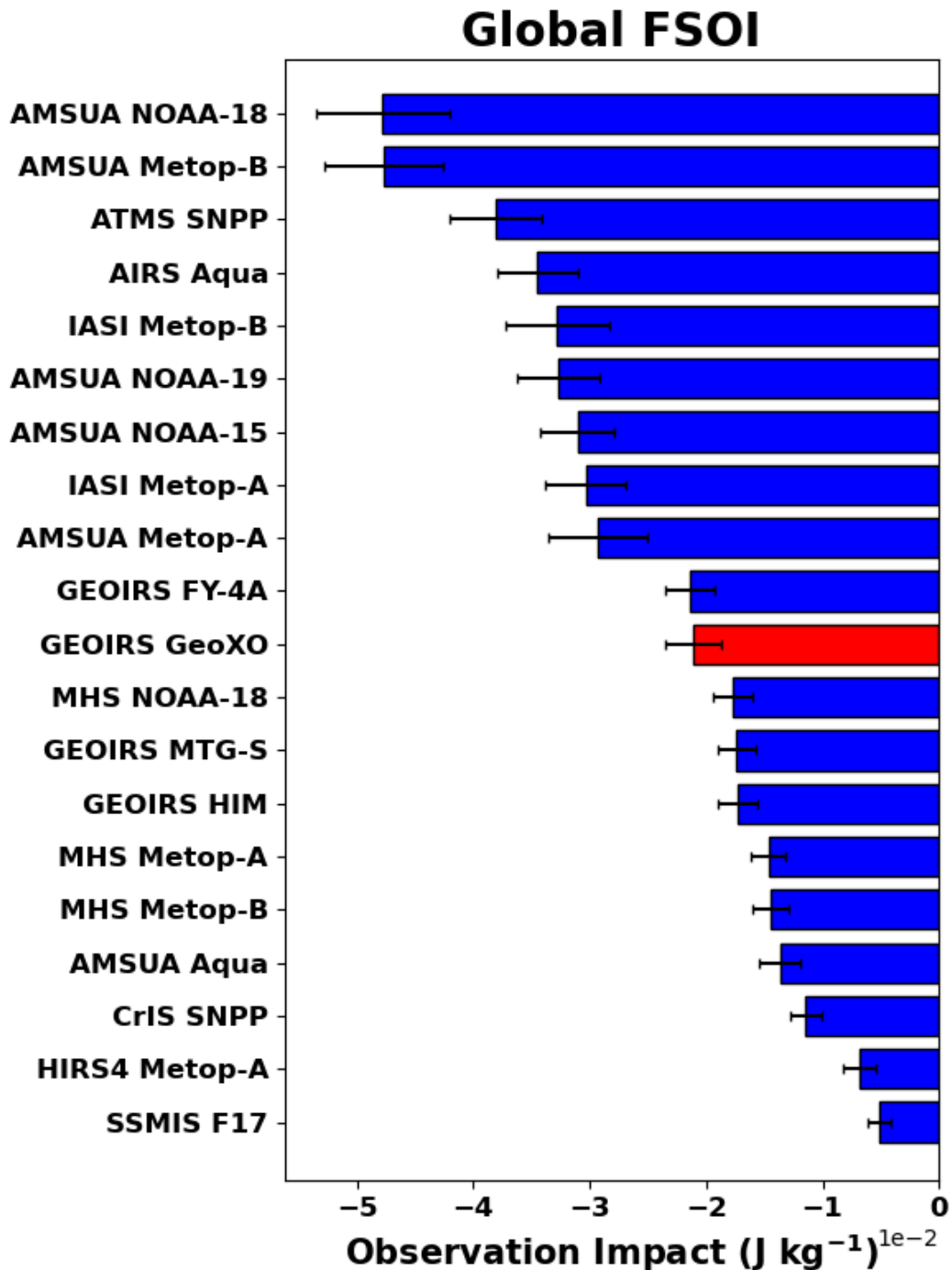


FIG. 11. FSOI per analysis as a function of satellite radiance instrument calculated globally for the 00 UTC analysis, in J kg^{-1} . The impact of the GEOIRS instruments was computed without the influence of the assimilated channels that are outside the specification of the proposed GXS instrument. Error bars indicate significance at the 90% level. The GXS instrument is highlighted in red.

However, the examination of the impact over the CONUS region and across all four synoptic times (00, 06, 12, and 18 UTC), shown in Figure 12, produces a different result. In this spatiotemporal domain, observations from the geostationary orbit have a stronger impact on the 24-hour forecast and the GXS provides a distinct observation impact among the infrared satellite radiances on moist energy error norm reduction and is well within the error bars of the estimate for ATMS SNPP in the top spot. Polar orbiters only observe a given location two times per day and many of their observations are outside of the CONUS region (Wang et al. 2021). They are therefore incapable of providing as much temporal information as an instrument directly overhead that provides valuable atmospheric sounding data nearly continuously. This temporal information is critical, allowing a strong observation impact on the 24 hour forecast error from the GXS instrument. Although the impact from the AMSU-A instruments may be underestimated for CONUS as was shown in Figure 1, there is potential from the GXS instrument to positively impact short-term weather forecasts and aid in decision-making by stakeholders.

7. Summary and Conclusions

The results of this study characterize some potential impacts from a "ring" of hyperspectral IR sounders on geostationary platforms with an emphasis on the proposed sounder on NOAA's GeoXO satellite at 105°W. This was done within the context of an OSSE with the implied caveats of an entirely simulated environment and the associated limitations. Radiances were simulated based on specifications for the IRS on the European MTG and the DAS was run using a hybrid 4DEnVar assimilation scheme that assumes hourly observation binning, coarser than the temporal resolution of the proposed GXS. The assimilated geostationary IR radiances did not include explicitly added errors so these results should be viewed as an upper limit on the utility of these observations.

The GXS and geostationary IR sounders more generally have the potential to provide new and important information content to numerical weather prediction systems by providing nearly continuous vertical profiling of key weather phenomena and processes. This would fill a knowledge gap left by current polar orbiting IR sounders and address needs identified by the WMO (WMO 2020) that may extend beyond NWP.

The assimilation of additional geostationary hyperspectral infrared radiances resulted in widespread improvements to the analysis temperature, humidity, and zonal wind. This error

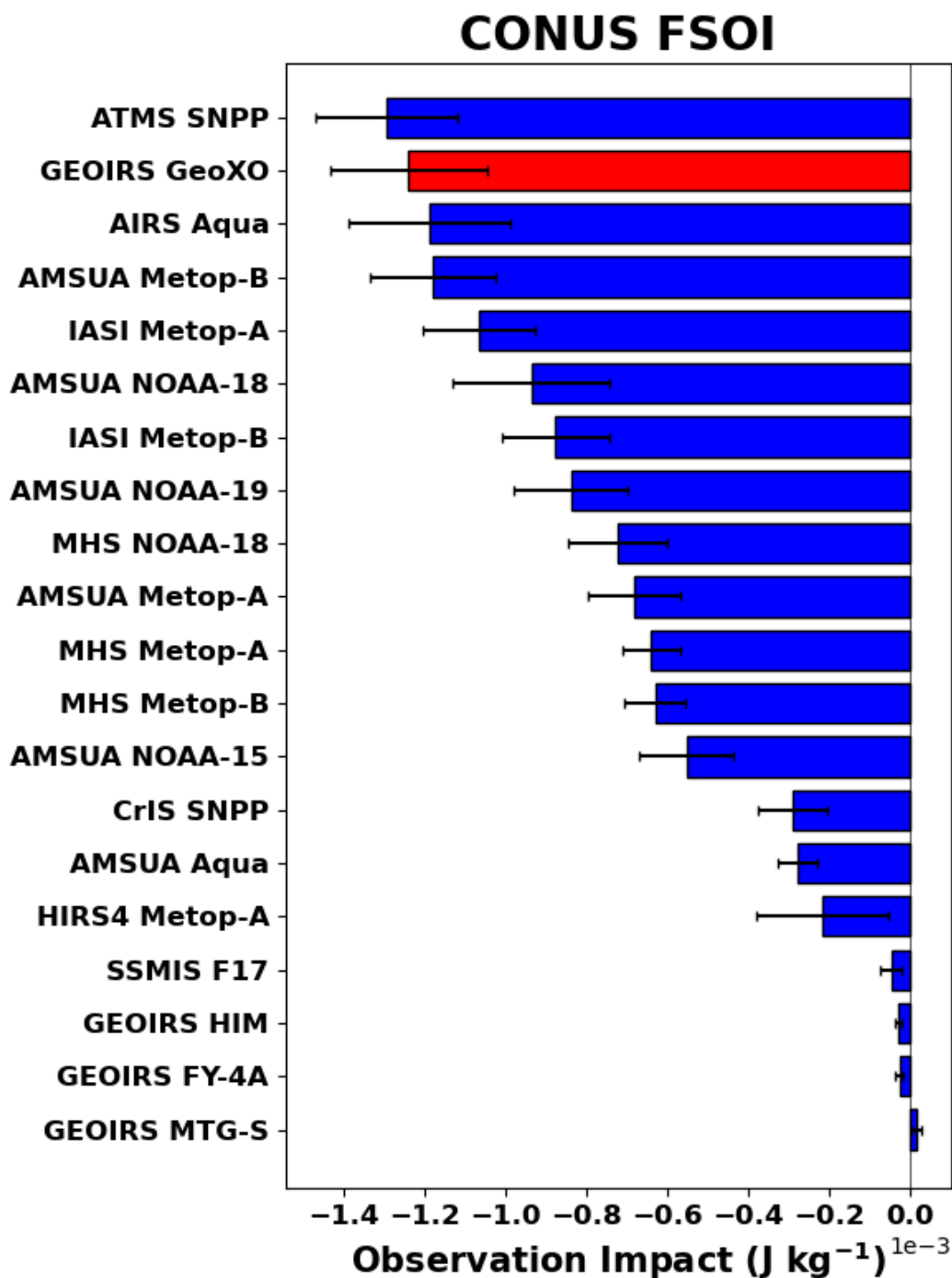


FIG. 12. Same as Figure 11, but computed over the CONUS domain and for the 00, 06, 12, and 18 UTC analysis cycles, in J kg⁻¹.

reduction primarily occurred in the tropics where geostationary instruments have the broadest span of observations. This included a modest temperature improvement equatorward of 30° with a degradation south of 30°S at upper levels, largely confined to the Pacific Ocean. Furthermore, the improved temporal resolution of vertical profiling lead to improved estimates of wind speed equatorward of the midlatitude jets. This improvement, combined with the effect on temperature and the direct impact of assimilating water vapor channels (through the Jacobian of brightness temperature with respect to humidity), contributed to improved estimates of specific humidity through improved tracer transport, with the largest impacts in the tropics between roughly 800 hPa and 300 hPa.

Improvements in the analysis resulted in improved initial conditions for the subsequent forecasts. Generally, the improved initial conditions drove significantly improved 24 - 48 hour forecasts. For temperature and zonal wind, statistically significant forecast improvements occurred throughout the tropospheric column, leading to improvements for numerical weather prediction in the first 1-2 days of simulation. In contrast, the tropospheric specific humidity improvement above approximately 800 hPa, important for dry air entrainment into clouds, extended longer into the forecast and was of stronger magnitude. However, lower tropospheric humidity forecasts were degraded in the 4-Sat experiment, related to greater complexity in infrared radiance assimilation over land due to larger surface heterogeneity and to issues with estimates over the cloud decks off the western coast of the United States. The errors over the stratocumulus cloud decks in the DAS, relative to the representation of clouds in the G5NR, are related to the parameterization choices made in the DAS and the difficulty the DAS has in representing sharp gradients.

The final evaluation metric examined here was the FSOI metric, which gives an estimate of the moist energy error norm reduction for a given observation type. This metric considers the 24 hour forecast error across multiple variables and therefore quantifies a broad understanding of the capability of individual observation types to impact forecast skill. Examining the impact of satellite radiance assimilation globally, polar orbiters, which are capable of observing the full assessed domain, outperformed instruments that are regionally focused, such as those on geostationary platforms. However, when focusing on the targeted domain of CONUS and examining the impact across the full diurnal cycle, the potential of a hyperspectral IR instrument on a geostationary

platform was apparent, with GXS being in the top cluster of radiance observations and having the largest impact on the 24 hour forecast error of all IR radiance types.

Several limitations of this work must be considered. One such limitation is that explicit errors have not been added to the GEOIRS observations. Since the GXS is still in development, the error magnitude is unknown and uncertainty exists in its determination. The above results are therefore an upper limit on the utility of the GXS and other GEOIRS instruments in reducing the analysis and forecast error. The channel range and ultimate selection for use in NWP is not yet determined and may also affect future results. Specifically, 20% of the assimilated channels used in this study are outside the current proposed spectral range of the GXS instrument. Efforts were made to limit the influence of these channels in this study by excluding results aloft of 100 hPa though some effects remain as the weighting functions of these channels extend downward to 300 hPa. The channel selection for NWP will necessarily be different. Additionally, the channels chosen for this study were assumed to be uncorrelated in the DAS solution, even though the real instrument is likely to suffer from error correlation and this source of error should be addressed before real data are assimilated.

One goal of new weather instruments is to improve the representation and forecast of weather phenomena in numerical weather prediction models. Through an evaluation using an OSSE, the capability of the proposed hyperspectral IR sounder on the GeoXO platform to make these improvements was assessed and found to have the potential to improve representations in the analysis, particularly in the tropics, and to reduce forecast error in the 24 - 48 hour time range. As the methodology to assimilate all-sky IR radiances matures, the assimilation of observations in cloudy regions will have the potential to produce even greater improvements as has been shown by studies assimilating cloud-cleared IR radiances (Wang et al. 2015; Reale et al. 2018; Wang et al. 2019; McGrath-Spangler et al. 2021; Ganeshan et al. 2022). Further evaluation of the capabilities of this new instrument type could include efforts to better exploit land and ozone sensitive channels that may reduce associated uncertainties. Upcoming updates to the GMAO OSSE system may further elucidate the potential of the GeoXO program.

Acknowledgments. The authors gratefully acknowledge allocations on the NASA High-End Computing resources. We thank Ron Errico for developing the baseline OSSE system. We also thank two anonymous reviewers who offered valuable feedback to improving this manuscript. Funding was provided by the NOAA and NASA GeoXO Project. All simulations were performed at the NASA Center for Climate Studies (NCCS) in Greenbelt, Maryland.

Data availability statement. The dataset on which this paper is based is too large to be retained or publicly archived with available resources. Documentation and methods used to support this study are available from Erica McGrath-Spangler at NASA/GMAO.

References

- Arnold, C. P., and C. H. Dey, 1986: Observing-systems simulation experiments: Past, present, and future. *Bulletin of the American Meteorological Society*, **67** (6), 687 – 695, [https://doi.org/10.1175/1520-0477\(1986\)067<0687:OSSEPP>2.0.CO;2](https://doi.org/10.1175/1520-0477(1986)067<0687:OSSEPP>2.0.CO;2), URL https://journals.ametsoc.org/view/journals/bams/67/6/1520-0477_1986_067_0687_ossepp_2_0_co_2.xml.
- Atlas, R., E. Kalnay, and M. Halem, 1985: Impact of satellite temperature sounding and wind data on numerical weather prediction. *Opt. Eng.*, **24**.
- Bacmeister, J. T., M. J. Suarez, and F. R. Robertson, 2006: Rain reevaporation, boundary layer–convection interactions, and pacific rainfall patterns in an agcm. *Journal of the Atmospheric Sciences*, **63** (12), 3383 – 3403, <https://doi.org/10.1175/JAS3791.1>, URL <https://journals.ametsoc.org/view/journals/atms/63/12/jas3791.1.xml>.
- Barahona, D., A. Molod, J. Bacmeister, A. Nenes, A. Gettelman, H. Morrison, V. Phillips, and A. Eichmann, 2014: Development of two-moment cloud microphysics for liquid and ice within the NASA Goddard Earth Observing System Model (GEOS-5). *Geosci. Model Dev.*, **7**, 1733–1766.
- Bauer, P., A. Thorpe, and G. Brunet, 2015: The quiet revolution of numerical weather prediction. *Nature*, **525** (7567), 47–55, <https://doi.org/https://doi.org/10.1038/nature14956>.
- Bessho, K., H. Owada, K. Okamoto, and T. Fujita, 2021: Himawari-8/9 follow-on satellite program and impacts of potential usage of hyperspectral ir sounder. *2021 IEEE International Geoscience*

and Remote Sensing Symposium IGARSS, 1507–1510, <https://doi.org/10.1109/IGARSS47720.2021.9553888>.

Cardinali, C., 2009: Monitoring the observation impact on the short-range forecast. *Quarterly Journal of the Royal Meteorological Society*, **135 (638)**, 239–250, <https://doi.org/https://doi.org/10.1002/qj.366>, URL <https://rmets.onlinelibrary.wiley.com/doi/abs/10.1002/qj.366>, <https://rmets.onlinelibrary.wiley.com/doi/pdf/10.1002/qj.366>.

Chen, Y., F. Weng, Y. Han, and Q. Liu, 2008: Validation of the community radiative transfer model by using cloudsat data. *Journal of Geophysical Research: Atmospheres*, **113 (D8)**, <https://doi.org/https://doi.org/10.1029/2007JD009561>, URL <https://agupubs.onlinelibrary.wiley.com/doi/abs/10.1029/2007JD009561>, <https://agupubs.onlinelibrary.wiley.com/doi/pdf/10.1029/2007JD009561>.

Cucurull, L., and S. P. F. Casey, 2021: Improved impacts in observing system simulation experiments of radio occultation observations as a result of model and data assimilation changes. *Monthly Weather Review*, **149 (1)**, 207 – 220, <https://doi.org/10.1175/MWR-D-20-0174.1>, URL <https://journals.ametsoc.org/view/journals/mwre/149/1/mwr-d-20-0174.1.xml>.

Diniz, F. L. R., and R. Todling, 2020: Assessing the impact of observations in a multi-year reanalysis. *Quarterly Journal of the Royal Meteorological Society*, **146 (727)**, 724–747, <https://doi.org/https://doi.org/10.1002/qj.3705>, URL <https://rmets.onlinelibrary.wiley.com/doi/abs/10.1002/qj.3705>, <https://rmets.onlinelibrary.wiley.com/doi/pdf/10.1002/qj.3705>.

Ehrendorfer, M., R. M. Errico, and K. D. Raeder, 1999: Singular-vector perturbation growth in a primitive equation model with moist physics. *Journal of the Atmospheric Sciences*, **56 (11)**, 1627 – 1648, [https://doi.org/10.1175/1520-0469\(1999\)056<1627:SVPGIA>2.0.CO;2](https://doi.org/10.1175/1520-0469(1999)056<1627:SVPGIA>2.0.CO;2), URL https://journals.ametsoc.org/view/journals/atsc/56/11/1520-0469_1999_056_1627_svpgia_2.0.co_2.xml.

Errico, R., and Coauthors, 2017: Description of the GMAO OSSE for weather analysis software package: Version 3. *NASA Technical Report Series on Global Modeling and Data Assimilation*, *NASA/TM-2017-104606*, **48**, 156 pp., URL <https://gmao.gsfc.nasa.gov/pubs/docs/Errico987.pdf>.

- Errico, R. M., and N. C. Privé, 2018: Some general and fundamental requirements for designing observing system simulation experiments (OSSEs). Tech. rep., WMO Report WWRP 2018-8, Geneva, Switzerland. URL <https://ntrs.nasa.gov/api/citations/20190025338/downloads/20190025338.pdf>.
- Errico, R. M., R. Yang, N. C. Privé, K.-S. Tai, R. Todling, M. E. Sienkiewicz, and J. Guo, 2013: Development and validation of observing-system simulation experiments at NASA's Global Modeling and Assimilation Office. *Quart. J. Roy. Meteor. Soc.*, **139**, 1162–1178.
- Eyre, J. R., and W. P. Menzel, 1989: Retrieval of Cloud Parameters from Satellite Sounder Data: A Simulation Study. *Journal of Applied Meteorology*, **28** (4), 267–275, [https://doi.org/10.1175/1520-0450\(1989\)028<textless{ }0267:ROCPFS\textgreater{ }2.0.CO;2](https://doi.org/10.1175/1520-0450(1989)028<textless{ }0267:ROCPFS\textgreater{ }2.0.CO;2).
- Ganeshan, M., O. Reale, E. McGrath-Spangler, and N. Boukachaba, 2022: Impact of assimilating adaptively thinned AIRS cloud-cleared radiances on the analysis of polar lows and mediterranean sea tropical-like cyclone in a global modeling and data assimilation framework. *Weather and Forecasting*, **37** (7), 1117 – 1134, <https://doi.org/10.1175/WAF-D-21-0068.1>, URL <https://journals.ametsoc.org/view/journals/wefo/37/7/WAF-D-21-0068.1.xml>.
- Gelaro, R., and Y. Zhu, 2009: Examination of observation impacts derived from observing system experiments (OSEs) and adjoint models. *Tellus A: Dynamic Meteorology and Oceanography*, **61** (2), 179–193, <https://doi.org/10.1111/j.1600-0870.2008.00388.x>, URL <https://doi.org/10.1111/j.1600-0870.2008.00388.x>, <https://doi.org/10.1111/j.1600-0870.2008.00388.x>.
- Gelaro, R., and Coauthors, 2015: Evaluation of the 7-km GEOS-5 nature run. *NASA Technical Report Series on Global Modeling and Data Assimilation, NASA/TM-2014-104606*, **36**, 305 pp., URL <https://gmao.gsfc.nasa.gov/pubs/docs/Gelaro736.pdf>.
- Guo, Q., and Coauthors, 2021: Spectrum calibration of the first hyperspectral infrared measurements from a geostationary platform: Method and preliminary assessment. *Quarterly Journal of the Royal Meteorological Society*, **147** (736), 1562–1583, <https://doi.org/https://doi.org/10.1002/qj.3981>, URL <https://rmets.onlinelibrary.wiley.com/doi/abs/10.1002/qj.3981>, <https://rmets.onlinelibrary.wiley.com/doi/pdf/10.1002/qj.3981>.

- Han, Y., P. van Delst, Q. Liu, F. Weng, B. Yan, R. Treadon, and J. Derber, 2006: Community radiative transfer model (CRTM): Version 1. *NOAA Tech. Rep. NESDIS*, **122**, 33 pp., URL <https://repository.library.noaa.gov/view/noaa/1157>.
- Hoffman, R. N., and R. Atlas, 2016: Future observing system simulation experiments. *Bulletin of the American Meteorological Society*, **97** (9), 1601 – 1616, <https://doi.org/10.1175/BAMS-D-15-00200.1>, URL <https://journals.ametsoc.org/view/journals/bams/97/9/bams-d-15-00200.1.xml>.
- Holdaway, D., R. Errico, R. Gelaro, and J. G. Kim, 2014: Inclusion of linearized moist physics in NASA's Goddard Earth Observing System data assimilation tools. *Mon. Wea. Rev.*, **142**, 414–433.
- Holmlund, K., and Coauthors, 2021: Meteosat Third Generation (MTG): Continuation and Innovation of Observations from Geostationary Orbit. *Bull. Amer. Meteor. Soc.*, **102** (5), E990 – E1015, <https://doi.org/10.1175/BAMS-D-19-0304.1>, URL <https://journals.ametsoc.org/view/journals/bams/102/5/BAMS-D-19-0304.1.xml>.
- Jones, T. A., S. Koch, and Z. Li, 2017: Assimilating synthetic hyperspectral sounder temperature and humidity retrievals to improve severe weather forecasts. *Atmospheric Research*, **186**, 9–25, <https://doi.org/https://doi.org/10.1016/j.atmosres.2016.11.004>, URL <https://www.sciencedirect.com/science/article/pii/S0169809516305750>.
- Kleist, D. T., D. F. Parrish, J. C. Derber, R. Treadon, W.-S. Wu, and S. Lord, 2009: Introduction of the GSI into the NCEP global data assimilation system. *Weather and Forecasting*, **24** (6), 1691–1705, <https://doi.org/10.1175/2009WAF2222201.1>, URL <https://doi.org/10.1175/2009WAF2222201.1>, <https://doi.org/10.1175/2009WAF2222201.1>.
- Langland, R. H., and N. L. Baker, 2004: Estimation of observation impact using the NRL atmospheric variational data assimilation adjoint system. *Tellus A: Dynamic Meteorology and Oceanography*, **56** (3), 189–201, <https://doi.org/10.3402/tellusa.v56i3.14413>, URL <https://doi.org/10.3402/tellusa.v56i3.14413>, <https://doi.org/10.3402/tellusa.v56i3.14413>.
- Lawrence, H., N. Bormann, I. Sandu, J. Day, J. Farnan, and P. Bauer, 2019: Use and impact of arctic observations in the ECMWF numerical weather prediction system. *Quarterly*

Journal of the Royal Meteorological Society, **145** (725), 3432–3454, <https://doi.org/https://doi.org/10.1002/qj.3628>, URL <https://rmets.onlinelibrary.wiley.com/doi/abs/10.1002/qj.3628>, <https://rmets.onlinelibrary.wiley.com/doi/pdf/10.1002/qj.3628>.

Li, Z., and Coauthors, 2018: Value-added impact of geostationary hyperspectral infrared sounders on local severe storm forecasts - via a quick regional OSSE. *Advances in Atmospheric Sciences*, **35** (10), 1217–1230, <https://doi.org/10.1007/s00376-018-8036-3>, URL <https://doi.org/10.1007/s00376-018-8036-3>.

Lin, S.-J., 2004: A "vertically Lagrangian" finite-volume dynamical core for global models. *Monthly Weather Review*, **132** (10), 2293–2307, [https://doi.org/10.1175/1520-0493\(2004\)132<2293:avlfdc>2.0.co;2](https://doi.org/10.1175/1520-0493(2004)132<2293:avlfdc>2.0.co;2).

McCarty, W., D. Carvalho, I. Moradi, and N. C. Privé, 2021: Observing system simulation experiments investigating atmospheric motion vectors and radiances from a constellation of 4–5- μm infrared sounders. *Journal of Atmospheric and Oceanic Technology*, **38** (2), 331 – 347, <https://doi.org/10.1175/JTECH-D-20-0109.1>, URL <https://journals.ametsoc.org/view/journals/atot/38/2/JTECH-D-20-0109.1.xml>.

McCarty, W., G. Jedlovec, and T. L. Miller, 2009: Impact of the assimilation of atmospheric infrared sounder radiance measurements on short-term weather forecasts. *Journal of Geophysical Research: Atmospheres*, **114** (D18), <https://doi.org/https://doi.org/10.1029/2008JD011626>, URL <https://agupubs.onlinelibrary.wiley.com/doi/abs/10.1029/2008JD011626>, <https://agupubs.onlinelibrary.wiley.com/doi/pdf/10.1029/2008JD011626>.

McGrath-Spangler, E. L., M. Ganeshan, O. Reale, N. Boukachaba, W. McCarty, and R. Gelaro, 2021: Sensitivity of low-tropospheric arctic temperatures to assimilation of airs cloud-cleared radiances: Impact on midlatitude waves. *Quarterly Journal of the Royal Meteorological Society*, **147** (741), 4032–4047, <https://doi.org/https://doi.org/10.1002/qj.4166>, URL <https://rmets.onlinelibrary.wiley.com/doi/abs/10.1002/qj.4166>, <https://rmets.onlinelibrary.wiley.com/doi/pdf/10.1002/qj.4166>.

McNally, A. P., P. D. Watts, J. A. Smith, R. Engelen, G. A. Kelly, J. N. Thépaut, and M. Matricardi, 2006: The assimilation of airs radiance data at ECMWF. *Quarterly Journal of the Royal Meteorological Society*, **132** (616), 935–957, <https://doi.org/https://doi.org/10.1002/qj.13206160101>.

org/10.1256/qj.04.171, URL <https://rmets.onlinelibrary.wiley.com/doi/abs/10.1256/qj.04.171>,
<https://rmets.onlinelibrary.wiley.com/doi/pdf/10.1256/qj.04.171>.

Molod, A., L. Takacs, M. Suarez, and J. Bacmeister, 2015: Development of the GEOS-5 atmospheric general circulation model: Evolution from MERRA to MERRA2. *Geoscientific Model Development*, **8** (5), 1339–1356.

Noh, Y.-C., A. H. N. Lim, H.-L. Huang, and M. D. Goldberg, 2020: Global forecast impact of low data latency infrared and microwave sounders observations from polar orbiting satellites. *Remote Sensing*, **12** (14), <https://doi.org/10.3390/rs12142193>, URL <https://www.mdpi.com/2072-4292/12/14/2193>.

Okamoto, K., and Coauthors, 2020: Assessment of the potential impact of a hyperspectral infrared sounder on the himawari follow-on geostationary satellite. *SOLA*, **16**, 162–168, <https://doi.org/10.2151/sola.2020-028>.

Privé, N. C., R. M. Errico, , and K.-S. Tai, 2014: The impact of increased frequency of rawinsonde observations on forecast skill investigated with an observing system simulation experiment. *Mon. Wea. Rev.*, **142**, 1823–1834, doi:10.1175/MWR-D-13-00237.1.

Privé, N. C., and R. M. Errico, 2013: The role of model and initial condition error in numerical weather forecasting investigated with an observing system simulation experiment. *Tellus*, **65A**, 21 740.

Privé, N. C., and R. M. Errico, 2019: Uncertainty of observation impact estimation in an adjoint model investigated with an observing system simulation experiment. *Monthly Weather Review*, **147** (9), 3191 – 3204, <https://doi.org/10.1175/MWR-D-19-0097.1>, URL <https://journals.ametsoc.org/view/journals/mwre/147/9/mwr-d-19-0097.1.xml>.

Privé, N. C., R. M. Errico, and A. E. Akkraoui, 2022: Investigation of the potential saturation of information from global navigation satellite system radio occultation observations with an observing system simulation experiment. *Monthly Weather Review*, **150** (6), 1293 – 1316, <https://doi.org/10.1175/MWR-D-21-0230.1>, URL <https://journals.ametsoc.org/view/journals/mwre/150/6/MWR-D-21-0230.1.xml>.

- Privé, N. C., R. M. Errico, and W. McCarty, 2021: The importance of simulated errors in observing system simulation experiments. *Tellus A*, **147**, 121–138, doi: 10.1080/16000870.2021.1886795.
- Putman, W. M., and S.-J. Lin, 2007: Finite-volume transport on various cubed-sphere grids. *J. Comput. Phys.*, **227**, 55–78.
- Reale, O., E. L. McGrath-Spangler, W. McCarty, D. Holdaway, and R. Gelaro, 2018: Impact of adaptively thinned air cloud-cleared radiances on tropical cyclone representation in a global data assimilation and forecast system. *Weather and Forecasting*, **33** (4), 909 – 931, <https://doi.org/10.1175/WAF-D-17-0175.1>, URL https://journals.ametsoc.org/view/journals/wefo/33/4/waf-d-17-0175_1.xml.
- Rienecker, M., and Coauthors, 2008: The GEOS-5 data assimilation system—documentation of versions 5.0. 1, 5.1. 0, and 5.2. 0. *NASA Tech. Memo*, **27**, 101 pp., URL http://gmao.gsfc.nasa.gov/pubs/docs/GEOS5_104606-Vol27.pdf.
- Schmit, T. J., J. Li, S. A. Ackerman, and J. J. Gurka, 2009: High-spectral- and high-temporal-resolution infrared measurements from geostationary orbit. *J. Atmos. Oceanic Technol.*, **26**, 2273–2292.
- Todling, R., and A. El Akkraoui, 2018: The GMAO Hybrid Ensemble-Variational Atmospheric Data Assimilation System: Version 2.0. *NASA Tech. Memo*, **50**, 184, URL <https://gmao.gsfc.nasa.gov/pubs/docs/Todling1019.pdf>.
- Velden, C., and Coauthors, 2005: Recent innovations in deriving tropospheric winds from meteorological satellites. *Bulletin of the American Meteorological Society*, **86** (2), 205 – 224, <https://doi.org/10.1175/BAMS-86-2-205>, URL <https://journals.ametsoc.org/view/journals/bams/86/2/bams-86-2-205.xml>.
- Wang, F., J. Li, T. J. Schmit, and S. A. Ackerman", 2007: Trade-off studies of a hyperspectral infrared sounder on a geostationary satellite. *Appl. Opt.*, **46** (2), 200–209, <https://doi.org/10.1364/AO.46.000200>, URL <http://www.osapublishing.org/ao/abstract.cfm?URI=ao-46-2-200>.
- Wang, P., J. Li, Z. Li, A. H. N. Lim, J. Li, and M. D. Goldberg, 2019: Impacts of observation errors on hurricane forecasts when assimilating hyperspectral infrared sounder radiances in partially cloudy skies. *Journal of Geophysical Research: At-*

Atmospheres, **124** (20), 10 802–10 813, <https://doi.org/https://doi.org/10.1029/2019JD031029>, URL <https://agupubs.onlinelibrary.wiley.com/doi/abs/10.1029/2019JD031029>, <https://agupubs.onlinelibrary.wiley.com/doi/pdf/10.1029/2019JD031029>.

Wang, P., Z. Li, J. Li, and T. J. Schmit, 2021: Added-value of geo-hyperspectral infrared radiances for local severe storm forecasts using the hybrid osse method. *Advances in Atmospheric Sciences*, **38** (8), 1315–1333, <https://doi.org/10.1007/s00376-021-0443-1>, URL <https://doi.org/10.1007/s00376-021-0443-1>.

Wang, P., and Coauthors, 2015: Assimilation of thermodynamic information from advanced infrared sounders under partially cloudy skies for regional nwp. *Journal of Geophysical Research: Atmospheres*, **120** (11), 5469–5484, <https://doi.org/https://doi.org/10.1002/2014JD022976>, URL <https://agupubs.onlinelibrary.wiley.com/doi/abs/10.1002/2014JD022976>, <https://agupubs.onlinelibrary.wiley.com/doi/pdf/10.1002/2014JD022976>.

WMO, 2020: Vision for the WMO integrated global observing system in 2040. URL https://library.wmo.int/doc_num.php?explnum_id=10278, 38 pp. pp.

Wu, W.-S., R. J. Purser, and D. F. Parrish, 2002: Three-dimensional variational analysis with spatially inhomogeneous covariances. *Monthly Weather Review*, **130** (12), 2905–2916, [https://doi.org/10.1175/1520-0493\(2002\)130<2905:TDVAWS>2.0.CO;2](https://doi.org/10.1175/1520-0493(2002)130<2905:TDVAWS>2.0.CO;2), URL [https://doi.org/10.1175/1520-0493\(2002\)130<2905:TDVAWS>2.0.CO;2](https://doi.org/10.1175/1520-0493(2002)130<2905:TDVAWS>2.0.CO;2), [https://doi.org/10.1175/1520-0493\(2002\)130<2905:TDVAWS>2.0.CO;2](https://doi.org/10.1175/1520-0493(2002)130<2905:TDVAWS>2.0.CO;2).

Yang, J., Z. Zhang, C. Wei, F. Lu, and Q. Guo, 2017: Introducing the new generation of Chinese geostationary weather satellites, Fengyun-4. *Bull. Amer. Meteor. Soc.*, **98**, 1637–1658.

Zapotocny, T. H., J. A. Jung, J. F. L. Marshall, and R. E. Treadon, 2007: A two-season impact study of satellite and in situ data in the NCEP global data assimilation system. *Weather and Forecasting*, **22** (4), 887 – 909, <https://doi.org/10.1175/WAF1025.1>, URL https://journals.ametsoc.org/view/journals/wefo/22/4/waf1025_1.xml.

Zapotocny, T. H., J. A. Jung, J. F. L. Marshall, and R. E. Treadon, 2008: A two-season impact study of four satellite data types and rawinsonde data in the NCEP global data assimilation system.

Weather and Forecasting, **23** (1), 80 – 100, <https://doi.org/10.1175/2007WAF2007010.1>, URL https://journals.ametsoc.org/view/journals/wefo/23/1/2007waf2007010_1.xml.

Zhou, D. K., and Coauthors, 2002: Thermodynamic product retrieval methodology and validation for nast-i. *Appl. Opt.*, **41** (33), 6957–6967, <https://doi.org/10.1364/AO.41.006957>, URL <http://www.osapublishing.org/ao/abstract.cfm?URI=ao-41-33-6957>.

Zhu, Y., and R. Gelaro, 2008: Observation sensitivity calculations using the adjoint of the gridpoint statistical interpolation (GSI) analysis system. *Mon. Wea. Rev.*, **136**, 335–351.